Inorganic Chemistry

Article

pubs.acs.org/IC

Construction of Polynuclear Lanthanide (Ln = Dy^{III}, Tb^{III}, and Nd^{III}) Cage Complexes Using Pyridine–Pyrazole-Based Ligands: Versatile Molecular Topologies and SMM Behavior

Sukhen Bala,[†] Mousumi Sen Bishwas,[‡] Bhaskar Pramanik,[§] Sumit Khanra,[§] Katharina M. Fromm,[∥] Pankaj Poddar,[‡] and Raju Mondal*[,†]

[†]Department of Inorganic Chemistry, Indian Association for the Cultivation of Science, Kolkata 700032, India

[‡]Physical & Materials Chemistry Division, CSIR-National Chemical Laboratory, Dr. Homi Bhabha Road, Pune 411008, India

[§]Department of Chemical Sciences, Indian Institute of Science Education and Research, Kolkata, Mohanpur 741246, India

[∥]Department of Chemistry, University of Fribourg, Chemin du Musée 9, CH-1700 Fribourg, Switzerland

Supporting Information

ABSTRACT: Employment of two different pyridyl–pyrazolyl-based ligands afforded three octanuclear lanthanide(III) (Ln = Dy, Tb) cage compounds and one hexanuclear neodymium(III) coordination cage, exhibiting versatile molecular architectures including a butterfly core. Relatively less common semirigid pyridyl–pyrazolyl-based asymmetric ligand systems show an interesting trend of forming polynuclear lanthanide cage complexes with different coordination environments around the metal centers. It is noteworthy here that construction of lanthanide complex itself is a challenging task in a ligand system as soft N-donor rich as pyridyl–pyrazol. We report herein some lanthanide complexes using ligand containing only one or two O-donors compare to five N-coordinating sites. The resultant multinuclear lanthanide complexes show interesting magnetic and spectroscopic features originating from different spatial arrangements of the metal ions. Alternating current (ac) susceptibility measurements of the two dysprosium complexes display frequency- and temperature-dependent out-of-phase signals in zero and 0.5 T direct current field, a typical characteristic feature of single-molecule magnet (SMM) behavior, indicating different energy reversal barriers due to different molecular topologies. Another aspect of this work is the occurrence of the not-so-common SMM behavior of the terbium complex, further confirmed by ac susceptibility measurement.

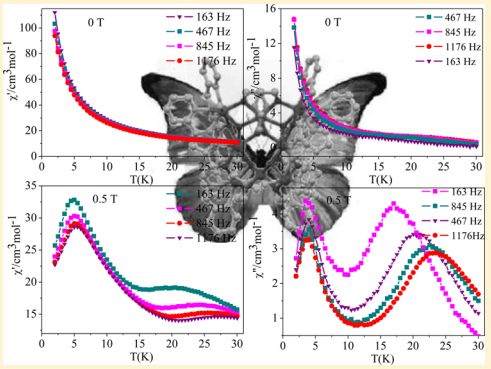

INTRODUCTION

Coordination cage compounds[1−5] are of unabated interest in SMMs,[2,3] magnetocaloric effects,[4] and in luminescence studies.[5] Among other applications, SMMs are of considerable promise as molecular spintronics devices for high-density data storage.[6] An escalating research interest has been developed to the design of lanthanide-based complexes, not only because of their intriguing structural architectures but also owing to their interesting magnetic[2−4,7−12] and luminescence properties.[5,7,10] Furthermore, highly luminescent complexes of Ln^{III} ions employ multidentate organic ligands as chromophore, which act as antennae to sensitize the weakly luminescent metal centers.[5] Hence, ligand design can play a crucial role not only to synthesize polynuclear cage complexes having versatile molecular topologies but also to significantly tune the magnetic and luminescent behaviors of the lanthanide complexes. Because of their significant anisotropy arising from large unquenched orbital angular momentum, lanthanide ions have become attractive candidates for SMMs.[8] Homometallic lanthanide compounds containing Dy^{III} have received considerable attention, and polynuclear complexes with variable nuclearity are known in literature.[3] Dy compounds are known to exhibit a slow relaxation, among which the Dy_5 square-based pyramid exhibits an energy barrier as high as 528 ± 11 K,[3a] clearly indicating that lanthanide compounds are highly promising for the development of SMMs with high-energy reversal barrier.

The final structural outcome can be engineered at a molecular level through subtle modification in the ligand backbone as it is known that the ligand influences the magnetic properties of paramagnetic complexes. There is a continuous need for the design of novel structures with versatile topologies that will improve the knowledge of structure–property relationships. In this regard, pyridyl–pyrazolyl-based frameworks have attracted significant attention in stabilizing polynuclear cage complexes,[1,13,14] with an overwhelming majority of transition metal-based complexes. However, even

Received: February 12, 2015
Published: August 25, 2015

DOI: 10.1021/acs.inorgchem.5b00334
Inorg. Chem. 2015, 54, 8197−8206

a cursory inspection would reveal that corresponding lanthanide chemistry is unexplored to date, except for a very few random examples.[5i−m] It is well-known that lanthanide ions have high affinity for hard donor atoms such as oxygen. Needless to mention, construction of lanthanide complex itself is a challenging task in a ligand system as soft N-donor rich as pyridyl−pyrazol. Notwithstanding these difficulties, the pyridyl−pyrazole-based ligands have a natural tendency to form polynuclear cages with metal ions, which are particularly important for SMM materials. This is particularly true considering the fact that the magnetic relaxation rates, the essence of SMMs, are extremely sensitive to tiny distortions of the coordination geometry in lanthanide complexes.[11] Our earlier report on pyridyl−pyrazolyl-based cages containing different coordination geometry of transition metals is highly relevant here.[14] The obvious question then arose as to whether lanthanide cage complexes could be produced with similar pyridyl−pyrazolyl-based ligands. Although, one potential obstacle to this strategy would be the coordinating nature of the ligands themselves with only one or two *hard* O-donors compare to five *soft* N-coordinating sites.

To study this question, we extend our work along these lines by employing two pyridyl−pyrazolyl-based ligands, namely, 3-(pyridin-2-yl)-*N*′-((pyridin-2-yl) methylene)-1*H*-pyrazole-5-carbohydrazide (H_2L_1) and *N*′-(2-hydroxybenzylidene)-3-(pyridin-2-yl)-1*H*-pyrazole-5-carbohydrazide (H_3L_2). Both ligands have two interrelated characteristic features, a semirigid backbone and the possibility to fulfill variable coordination modes, so that, depending on the coordination requirements, the ligands adopt different conformations via bending, stretching, or twisting of the rings. We envisioned that such a unique blend of asymmetric nature, conformational freedom as well as coordination flexibility of the semirigid ligands may direct the synthesis of polynuclear lanthanide complexes. Indeed, four new polynuclear lanthanide (III) (Ln = Dy^{III}, Tb^{III} and Nd^{III}) cage complexes of versatile molecular topologies were obtained using two pyridyl−pyrazolyl-based asymmetric, semirigid ligands. Their SMM nature and luminescence properties further validate the usefulness of this type of ligands for the study of lanthanide chemistry.

EXPERIMENTAL SECTION

All reagents used in the present work were obtained from commercial sources and were used without further purification unless otherwise stated. Fourier transform IR spectra were obtained on a Nicolet MAGNA-IR 750 spectrometer with samples prepared as KBr pellets. C, H, and N microanalyses were performed with a 2400 Series-II CHN Analyzer; Perkin−Elmer, USA, and UV−visible studies were performed in PerkinElmer Lambda 950 UV−vis instrument. Magnetic data of polycrystalline samples were collected by MPMS (Evercool, 7 T) by Quantum Design, and ^{1}H NMR was performed by Bruker Spectrometer operating at 400 MHz in deuterated dimethyl sulfoxide solvent. The photoluminescence measurements of solid samples were performed with the Horiba Jobin Yvon Fluoromax-3 spectrometer using steady-state 450 W Xe lamps as the excitation source, and excitation of the samples was done in UV region at 270 nm. Mass spectra were recorded on a Q-ToF Micro YA263 high resolution (Waters Corporation) mass spectrometer by positive ion mode electrospray ionization and the spectra were collected in methanol and water (1:1).

Synthesis of H_2L_1. The ligand 3-(pyridin-2-yl)-*N*′-((pyridin-2-yl)methylene)-1*H*-pyrazole-5-carbohydrazide (H_2L_1) was synthesized by refluxing 3-(pyridin-2-yl)-1*H*-pyrazole-5-carbohydrazide (0.203 g, 1.0 mmol) and 2-pyridinecarboxaldehyde (0.107 g, 1.0 mmol) in ethanol at 80 °C for 6 h using acetic acid as catalyst. After the solution cooled, a white precipitate formed, which was filtered and dried. (Yield: 77% based on carbohydrazide). Anal. Calcd for $C_{15}H_{12}N_6O$ (H_2L_1) (%): C, 61.64; H, 4.10; N, 28.76. Found: C, 61.67; H, 4.05; N, 28.67. IR (400−4000 cm^{-1}): 3436(b), 3299(s), 3074(s), 1674(s), 1533(s), 1226(s) . ^{1}H NMR (500 MHz, [$(CD_3)_2SO$], δ): 14.174 (s, 1H, pyz−H), 12.096 (s, 1H, NH), 8.650 (s, 1H, imine-H), 7.385−7.998 (8H, py-H). Electrospray ionization mass spectrometry (ESI-MS) *m*/*z* (M + H): 293.1258

Synthesis of H_3L_2. The ligand *N*′-(2-hydroxybenzylidene)-3-(pyridin-2-yl)-1*H*-pyrazole-5-carbohydrazide (H_3L_2) was synthesized by refluxing 3-(pyridin-2-yl)-1*H*-pyrazole-5-carbohydrazide(0.203 g, 1.0 mmol) and salicylaldehyde(0.122 g, 1.0 mmol) in ethanol at 80 °C for 6 h using acetic acid as catalyst. After the solution cooled, a light yellow precipitate formed, which was filtered and dried in air. (Yield: 82% based on carbohydrazide) Anal. Calcd for $C_{16}H_{13}N_5O_2$ (H_3L_2) (%):C, 62.54; H, 4.24; N, 22.27. Found: C, 62.25; H, 4.32; N, 22.53. IR (400−4000 cm^{-1}): 3429(b), 3275(s), 2995(s), 1654(s), 1614(s), 1541(s), 1467(s), 1400(s), 1274(s), 1205(s), 1163(s). ^{1}H NMR (500 MHz, [$(CD_3)_2SO$], δ) 14.169(s, 1Hpyz-H), 12.184(s, 1H, NH), 11.427(s, 1H, phenolic-OH), 8.797(s, 1H, imine-H), 7.329−7.983 (4H, py-H), 6.895−7.312 (4H, Ar−H). ESI-MS *m*/*z* (M + H): 308.

Synthesis of Complex 1 ($[Dy^{III}_8(\mu_3\text{-}OH)_4(L_1)_4(DEA)_4Cl_4]$). H_2L_1 (0.0292 g, 0.1 mmol), $DyCl_3{\cdot}6H_2O$ (0.0377g, 0.1 mmol), and diethanolamine (DEA, 0.021 g, 0.2 mmol) were dissolved in a solvent mixture containing 3 mL of methanol and 3 mL of dimethylformamide (DMF). Trimethylamine (0.02 g, 0.2 mmol) was used as base, and the mixture was stirred for half an hour and then heated in an oil bath at 80 °C for 6 h. The yellow solution was filtered after it cooled, and the solution was kept undisturbed for crystallization. After one week rod-shaped yellow crystals of complex **1** were obtained, which were suitable for X-ray data collection, washed with small amount of methanol, and dried. (Yield: 78%). Anal. Calcd for **1** (%): C, 29.63; H, 2.79; N, 12.45. Found: C, 29.32; H, 2.87; N, 12.14. IR (400−4000 cm^{-1}): 3394(b), 2933(mb), 2846(ms), 1656(s), 1596(s), 1512(s), 1467(s), 1434(s), 1386(s), 1309(s), 1251(s), 1157(s), 1049(s).

Synthesis of Complex 2 ($[Tb^{III}_8(\mu_3\text{-}OH)_4(L_1)_4(DEA)_4Cl_4]$). H_2L_1 (0.0292 g, 0.1 mmol), $TbCl_3{\cdot}6H_2O$ (0.0374g, 0.1 mmol), and DEA (0.021 g, 0.2 mmol) were dissolved in a solvent mixture containing 3 mL of methanol and 3 mL of DMF. Triethylamine (0.02 g, 0.2 mmol) was used as base, and the mixture was stirred for half an hour and then heated in an oil bath at 80 °C for 6 h. The yellow solution was filtered after it cooled, and the solution was kept undisturbed for crystallization. Rod-shaped yellow crystals of complex **2** were obtained within 5 d that were suitable for X-ray data collection, washed with small amount of methanol, and dried. (Yield: 77%). Anal. Calcd for **2** (%): C, 29.85; H, 2.61; N, 12.83. Found: C, 30.17; H, 2.72; N, 12.47. IR (400−4000 cm^{-1}): 3382(b), 3249(ms), 2844(s), 1656(s), 1596(s), 1566(s), 1506(s), 1465(s), 1433(s), 1386(s), 1348(s), 1309(s), 1249(s), 1157(s), 1047(s).

Synthesis of Complex 3 ($[Dy^{III}_8(\mu_3\text{-}OH)_4(L_2)_6(DMF)_4(H_2O)_8]$). H_3L_2 (0.0307 g, 0.1 mmol) and $DyCl_3{\cdot}6H_2O$ (0.0377 g, 0.1 mmol) were dissolved in a solvent mixture containing 3 mL of methanol and 3 mL of DMF. Triethylamine (0.02 g, 0.2 mmol) was used as base, and the mixture was stirred for half an hour and then heated in an oil bath at 80 °C for 6 h. The light brown solution was filtered and kept undisturbed for crystallization. Needle-shaped brown crystals of complex **3** were obtained within two that were suitable for X-ray data collection, washed with small amount of methanol, and dried. (Yield: 72%). Anal. Calcd for **3** (%): C, 35.64; H, 3.13; N, 13.09. Found: C, 35.81; H, 3.16; N, 12.91. IR (400−4000 cm^{-1}): 3377(vb), 2927(ms), 1658(s), 1602(s), 1442(s), 1371(s), 1261(s), 1201(s), 1153(s), 1103(s), 1043(s).

Synthesis of Complex 4 ($[Nd^{III}_6(\mu_3\text{-}OH)_2(L_2)_4(L_2H)_2(DMF)_2(H_2O)_5]$). H_3L_2 (0.0307 g, 0.1 mmol) and $NdCl_3{\cdot}6H_2O$ (0.025 g, 0.1 mmol) were dissolved in a solvent mixture containing 3 mL of methanol and 3 mL of DMF. Triethylamine (0.02 g, 0.2 mmol) was used as base, and the mixture was stirred for half an hour and then heated in an oil bath at 80 °C for 6 h. The light brown solution was filtered and kept undisturbed for crystallization. Needle-shaped brown crystals of complex **4** were obtained within two weeks

DOI: 10.1021/acs.inorgchem.5b00334
Inorg. Chem. 2015, 54, 8197−8206

that were suitable for X-ray data collection, washed with small amount of methanol, and dried. (Yield: 67%). Anal. Calcd for **4** (%): C, 41.78; H, 3.65, 15.43. Found: C, 41.85; H, 3.81; N, 15.35. IR (400−4000 cm^{-1}): 3386(b), 2925(ms), 1654(s), 1604(s), 1544(s), 1471(s), 1438(s), 1386(s), 1296(s), 1249(s), 120(s)1, 1153(s), 1103(s), 1039(s).

X-ray Crystallography. X-ray diffraction intensities for compounds **1**−**4** were collected at 120 K on Bruker APEX-2 CCD and diffractometer using Mo Kα radiation and processed using SAINT. The structures were solved by direct methods in SHELXS and refined by full matrix least-squares on F^2 in SHELXL.[15] Crystallographic data are summarized in Table S1, and additional crystallographic information is available in the Supporting Information.

RESULTS AND DISCUSSION

Synthesis. The ligands can be prepared in high yields by Schiff base reactions of 3-(pyridin-2-yl)-1*H*-pyrazole-5-carbohydrazide with 2-pyridinecarboxaldehyde or salicylaldehyde in ethanol using acetic acid as catalyst. The lanthanide complexes were synthesized under similar conditions using $LnCl_3{\cdot}6H_2O$ (Ln = Dy, Tb, Nd) and H_2L_1 or H_3L_2 at 80 °C. When $DyCl_3{\cdot}6H_2O$ reacted with the ligand H_2L_1 in the presence of DEA in a 1:1:2 molar ratio and with NEt_3 as base, crystals of $[Dy^{III}{}_8(\mu_3\text{-}OH)_4(L_1)_4(DEA)_4Cl_4]$ (**1**) were obtained. The homologue $[Tb^{III}{}_8(\mu_3\text{-}OH)_4(L_1)_4(DEA)_4Cl_4]$) (**2**) was obtained when $TbCl_3{\cdot}6H_2O$ was used under similar reaction conditions. The reaction of $DyCl_3{\cdot}6H_2O$ with 1 equiv of ligand H_3L_2 in DMF and NEt_3 as base afforded the crystals of $[Dy^{III}{}_8(\mu_3\text{-}OH)_4(L_2)_6(DMF)_4(H_2O)_8]$ (**3**). Changing the lanthanide ion to $NdCl_3{\cdot}6H_2O$ leads to $[Nd^{III}{}_6(\mu_3\text{-}OH)_2(L_2)_4(L_2H)_2(DMF)_2(H_2O)_5]$ (**4**). All the complexes are characterized by elemental analysis, IR spectroscopy, and X-ray single-crystal diffraction analyses.

Description of Molecular Structures. Single-crystal X-ray analysis reveals that **1** crystallizes in the monoclinic *C*2/*c* space group and consists of a discrete neutral $[Dy^{III}{}_8(\mu_3\text{-}OH)_4(L_1)_4(DEA)_4Cl_4]$ entity and methanol molecules as cocrystallizing solvent. The molecular structure of **1** without the solvent molecules is depicted in Figure 1, and selected geometrical

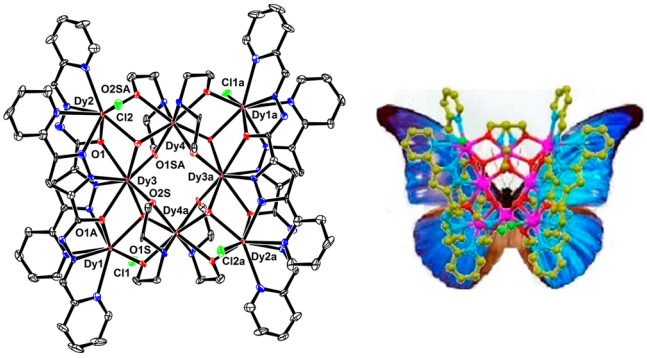

Figure 1. Perspective view of **1** with thermal ellipsoids at the 50% probability level (left) and butterfly topology (right). Hydrogen atoms are omitted for clarity.

parameters are provided in Table S2. Eight Dy^{III} ions are held together by four μ_3-OH^- ligands (O1WS, O2WS, and symmetry equivalents) to form the $[Dy_8(OH)_4]$ core as shown in Figure 2, which is composed of four triangular Dy_3 units sharing vertices with Dy···Dy separations of 3.820 Å for Dy2···Dy4, 3.764 Å for Dy3···Dy4, and 3.848 Å for Dy1···Dy4. These μ_3-OH^- centered triangular units are similar to those of earlier reported Dy(III) compounds.[3] In the $\{Dy_3(\mu_3\text{-}OH)\}$

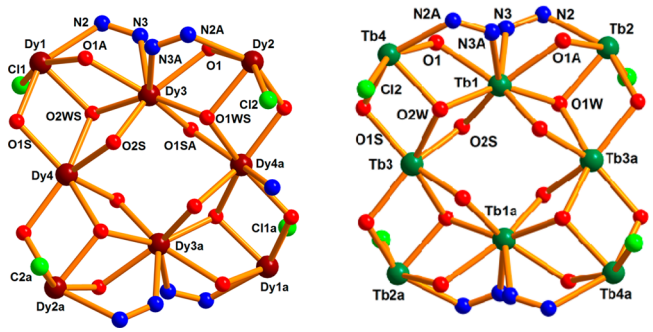

Figure 2. Representation of the $Dy^{III}{}_8$ (left) and $Tb^{III}{}_8$ core (right) in **1** and **2**, respectively.

cores defined by the Dy−O bonds, Dy−O−Dy angles, and Dy···Dy separations, the geometric parameters with Dy−O bonds varying from 2.352(6) to 2.435(6) Å, the Dy−O−Dy angles span from 101.2(2)° to 110.8(2)°, and Dy···Dy separations range from 3.7323(11) Å to 3.8792(11) Å. Each triangular unit is further connected by eight μ_2-η^2 alkoxide oxygen atoms (O1S, O2S, and symmetry equivalents) from the four deprotonated diethanolamine coligands, where the Dy−O bond lengths are found to lie in the range from 2.253(6) to 2.368(6) Å and are in agreement with the literature.[3,9−12] Four amide oxygen atoms (O1, O1A, and symmetry equivalents) of the dianionic ligand $\{L_1\}$ are also bridging in a μ_2-η^2 fashion, connecting the Dy^{III} centers. Peripheral ligations are provided by the nitrogen atoms from the pyridine and pyrazole motifs. Dy1, Dy2, and their symmetry equivalents are further coordinated by terminal Cl^- ions with Dy−Cl bond lengths of 2.674(2) and 2.703(2) Å.

The major impetus for this work was to validate the usefulness of the pyridyl−pyrazole-based ligands in designing polynuclear lanthanide complexes with different coordination environments. We are gratified to note that our assumptions were correct. The dysprosium ions exhibit different coordination environments; Dy1 and Dy2 are eight-coordinated with a $DyO_3N_4Cl_1$ coordination motif, and the geometry around them can be best described as distorted square antiprism, whereas Dy3 and Dy4 are also eight-coordinated but in DyO_6N_2 coordination motif with a bicapped trigonal prism geometry, as represented in Figure 3. As far as topology is concerned, the

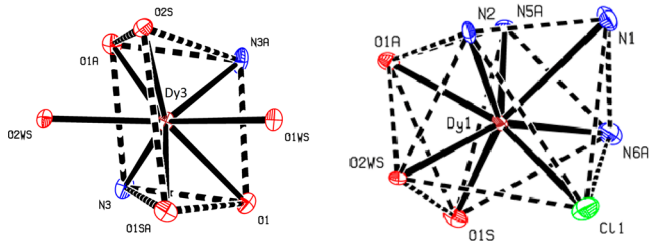

Figure 3. Representations of bicapped trigonal prism and distorted square antiprismatic geometry around Dy in **1**.

Dy_8 core closely resembles a butterfly (Figure 1) wherein the orientation of ligands can be envisaged as wings and Dy4 coordinated to the DEA-part as body.

Complex **2** also crystallizes in the monoclinic *C*2/*c* space group, and the lattice consists of a discrete neutral $[Tb^{III}{}_8(\mu_3\text{-}OH)_4(L_1)_4(DEA)_4Cl_4]$ molecule. The molecular structure of **2** is isostructural to that of **1** including the butterfly core shown in

DOI: 10.1021/acs.inorgchem.5b00334
Inorg. Chem. 2015, 54, 8197−8206

Figure S4, and selected geometrical parameters are represented in Table S2. The $\{Tb_3(\mu_3\text{-}OH)\}$ units display Tb−O bonds in the range from 2.336(6) to 2.425(5) Å, the Tb−O−Tb angles vary from 101.6(2)° to 110.1(2)°, and the Tb···Tb separations range from 3.735 to 3.889 Å. The Tb−O bond distances in **2** are in the range of 2.251(5)−2.501(5) Å, while Tb−N_{py} and Tb−N_{pz} are in the range of 2.515(7)−2.777(7) Å and 2.411(7)−2.465(7) Å, respectively. The bond lengths are comparable to those of previously reported Tb^{III} complexes.[6,10a] The Tb−Cl bond lengths are 2.645(3) and 2.685(3) Å. The different coordination environments around the Tb^{III} centers are reminiscent of the Dy compound **1**.

Both Tb2 and Tb4 are eight-coordinated with a $TbO_3N_4Cl_1$ coordination motif, and the geometry around them can be best described as distorted square antiprismatic, whereas Tb1 and Tb3 are also eight-coordinated but with a TbO_6N_2 coordination motif with a bicapped trigonal prism geometry as shown in Figure S5. The $\{Tb^{III}{}_8\}$ core is presented in Figure 2.

In contrast to **1** and **2**, complex **3** crystallizes in the triclinic $P\bar{1}$ space group and consists of a discrete $[Dy^{III}{}_8(\mu_3\text{-}OH)_4(L_2)_6(DMF)_4(H_2O)_8]$ (**3**) molecule. Replacement of the terminal pyridyl group with a salicylic phenolic group in the ligand system did bring some drastic changes in the crystal structure of **3**. The Dy_8 core of compound **3** adopts a staircase-type arrangement. The molecular structure of **3** is presented in Figure 4, and selected geometrical parameters are given in

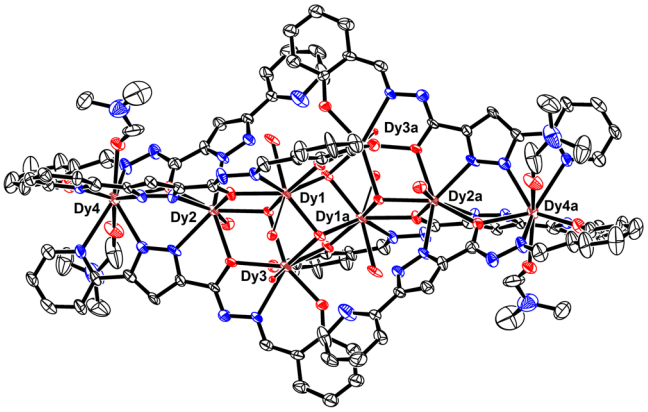

Figure 4. Perspective view of **3** with thermal ellipsoids at the 50% probability level. Hydrogen atoms are omitted for clarity.

Table S2. Inspection of molecular structure indicates that six Dy^{III} ions are held together by four μ_3-OH^- and six μ_2-OR-ligands $\{L_2\}$, where the $[Dy_6(\mu_3\text{-}OH)_4(\mu_2\text{-}OR)_6]^{8+}$ core consists of two $[Dy_3(\mu_3\text{-}OH)(\mu_2\text{-}OR)_2]$ triangular units in an "edge-to-edge" arrangement linked by two μ_3-OH^- ions and two deprotonated alcohol oxygen atoms from the $\{L_2\}$ ligands. The dysprosium triangles Dy1Dy2Dy3 and symmetry equivalent are linked by μ_3-OH^- ions (O1S and counterpart) capping above and below the plane of the triangle, with Dy···Dy distances of 3.927, 3.9530, and 3.722 Å. Two sides of the triangles are further bridged by two deprotonated alkoxo oxygen atoms (O2 and symmetry equivalent), while the remaining side is coordinated by a μ_3-OH^- ion (O6S and counterpart). The equivalent oxygen atoms (O6S) together with two alkoxo oxygen atoms link the two dysprosium triangular units, which results in an edge-to-edge arrangement of the dysprosium triangles. Dy2 and symmetry equivalents are further bridged to Dy4 and symmetry equivalent, respectively, via two pyrazolyl nitrogen atoms (N2, N3, and symmetry equivalent) in a bidentate fashion alongside an oxygen atom (O1A and counterpart) in μ_2-η^2 leading to the Dy^{III}_8 cage complex; the core structure is presented in Figure 5. Note that the topology in **3** is quite different from the Dy_8 cage in **1**. The coordination is completed by oxygen atoms from the water and DMF solvent molecules.

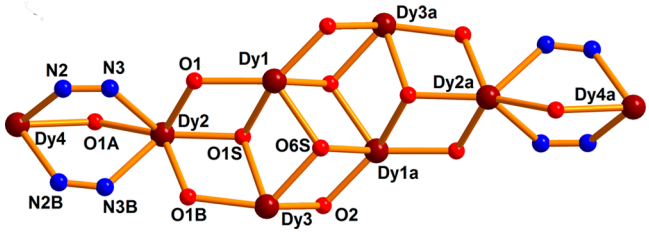

Figure 5. Representation of the Dy^{III}_8 core in **3**.

Alternatively, the core structure of **3** can be described as four incomplete heterocubane entities "Dy_3O_4", which miss one Dy ion to complete the heterocubane entities and are fused to each other via Dy_2O_2-faces. The "terminal" Dy2 atom (and its symmetry equivalent) is further connected to Dy4 via two bridging N atoms of the pyrazolyl ligands and a bridging O atom.

The values of the Dy−O and Dy−N bond lengths cover the ranges from 2.221(8)−2.491(6) and 2.386(8)−2.690(9) Å, respectively. The Dy−O−Dy angles are comprised between 99.9(2)° and 123.2(3)°. In an excellent agreement with our assumption, the dysprosium ions display again different coordination environments. Dy1 and Dy3 possess an eight-coordinated DyO_7N_1 motif, and the geometry around them can be best described as bicapped trigonal prism, whereas Dy2 has a DyO_5N_3 coordination motif displaying bicapped trigonal prism geometry. The geometry around Dy4 and its symmetry equivalent is different with a nine-coordinated DyO_4N_5, which can best be described as monocapped square antiprismatic. The coordination spheres of the dysprosium ions are illustrated in Figure 6.

Introduction of neodymium as lanthanide ion results in an interesting cage complex with a Nd_6 core, instead of an octanuclear core as observed earlier for **1**−**3**. It is noteworthy here that, for a given ligand, lanthanide complexes usually adopt a similar metal core. Complex **4** crystallizes in the hexagonal $P3_221$ space group and consists of a discrete neutral $[Nd^{III}{}_6(\mu_3\text{-}OH)_2(L_2)_4(L_2H)_2(DMF)_2(H_2O)_5]$ unit, as well as water and DMF molecules as solvents of crystallization. The molecular structure of the cage compound of **4** is presented in Figure 7, and metrical parameters are listed in Table S2. Single-crystal X-ray analysis of **4** reveals that four symmetry-independent Nd^{III} ions are held together by two μ_3-OH^- ligands (O1W and its symmetry equivalent) and four μ_2-OR^- ligands $\{L_2\}$, where the $[Nd_4(\mu_3\text{-}OH)_2(\mu_2\text{-}OR)_6]^{4+}$ core consists of two $[Nd_3(\mu_3\text{-}OH)(\mu_2\text{-}OR)_3]$ triangular units sharing the edge between Nd1 and Nd2 ions leading to a Nd_6 core. Nd1, Nd2, Nd3, and Nd3A linked by μ_3-OH^-ions atom are capped above and below the plane of the triangle, with Nd···Nd bond distances in the range of 3.740−4.173 Å and a body−body distance of 4.066 Å. Nd3 and its symmetry equivalent are further bridged to Nd4 and its symmetry equivalent, respectively, via two pyrazolyl nitrogen atoms (N2, N3, and symmetry equivalents) in a bidentate fashion alongside with an oxygen atom (O1A and

DOI: 10.1021/acs.inorgchem.5b00334
Inorg. Chem. 2015, 54, 8197−8206

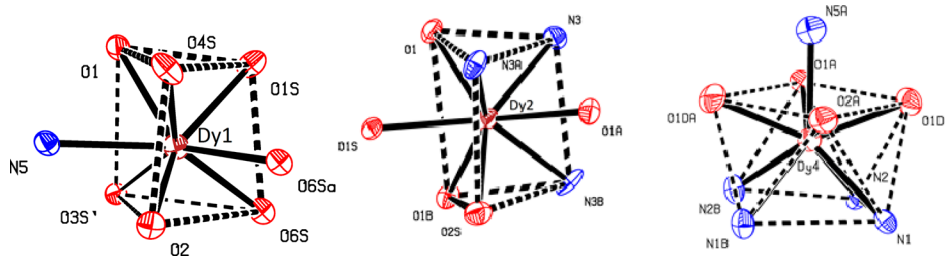

Figure 6. Representations of bicapped trigonal prism and monocapped square antiprismatic geometry around Dy in **3**.

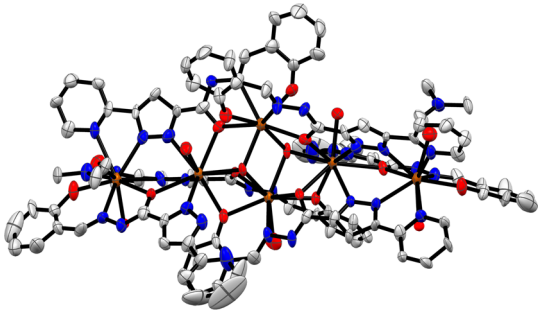

Figure 7. Perspective view of **4** with thermal ellipsoids at the 50% probability level. Hydrogen atoms are omitted for clarity.

counterpart) in μ_2-η^2 fashion leading to the Nd^{III}_6 core as shown in Figure 8. The coordination is completed by oxygen

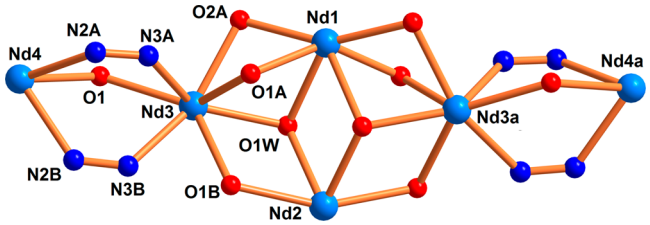

Figure 8. Representation of the Nd^{III}_6 core in **4**.

atoms from the water and DMF solvent molecules. The values of the Nd−O and Nd−N bond lengths cover the ranges of 2.297(9)−2.609(8) and 2.53(1)−2.276(1) Å, respectively. The Nd−O−Nd angles are in the range of 96.9(3)−130.8(8)°. Nd1 and Nd3 are nine-coordinated with an O_7N_2 and an O_6N_3 coordination motif, respectively, and the geometry can best be described as monocapped square antiprismatic.

In contrast, Nd2 and Nd4 are eight- and nine-coordinated with an O_6N_2 and an O_5N_4 coordination motif, respectively. The coordination spheres of the neodymium ions are illustrated in Figure 9.

Magnetic Properties. Variable-temperature direct current (dc) magnetic susceptibility data for compounds **1** (Dy_8Cl_4), **2** (Tb_8Cl_4), **3** (Dy_8), and **4** (Nd_6) were collected on powdered microcrystalline samples over a temperature range from 5 to 300 K and under an applied field of 0.5 T. The magnetic measurement on **1** reveals that the $\chi_M T$ value at 300 K is 105.95 cm^3 K mol^{-1}, which is somewhat smaller than the theoretical value of 113.36 cm^3 K mol^{-1} expected for eight noninteracting Dy^{III} ions (S = 5/2, L = 5, $^6H_{15/2}$, g = 4/3: C = 14.17 cm^3 K mol^{-1}).[8] When cooled, the $\chi_M T$ product decreases gradually to reach 98.8 cm^3 K mol^{-1} at 30 K and then decreases continuously to a value of 90.83 cm^3 K mol^{-1} at 10 K. The $\chi_M T$ versus T plot is shown in Figure 10. This may indicate the

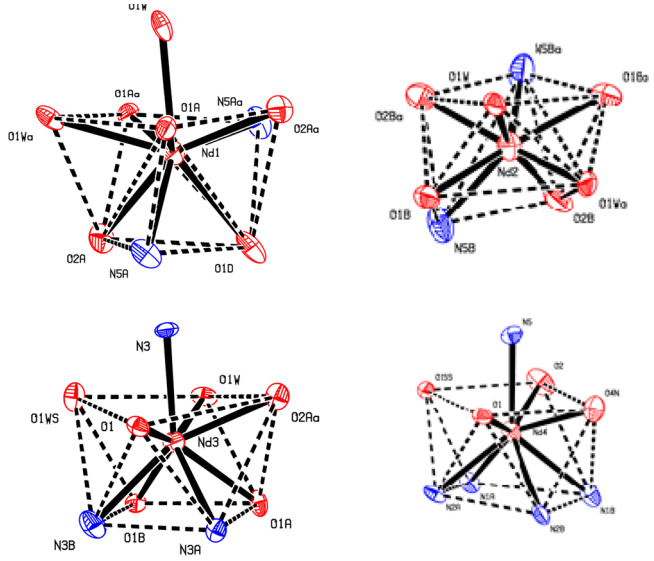

Figure 9. Representations of distorted square antiprismatic and monocapped square antiprismatic geometry around Nd in **4**.

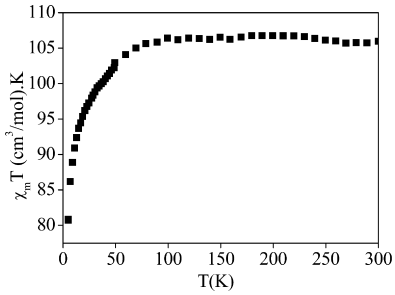

Figure 10. $\chi_M T$ vs T plot for complex **1**.

presence of weak antiferromagnetic interactions between the Dy^{III} ions. The $\chi_M T$ value of **3** at 300 K is 103.13 cm^3 K mol^{-1}, which is somewhat smaller than the theoretical value of 113.36 cm^3 K mol^{-1} expected for eight noninteracting Dy^{III} ions. When cooled, the $\chi_M T$ product decreases gradually to reach 95.0 cm^3 K mol^{-1} at 30 K and then decreases continuously to a value of 86.75 cm^3 K mol^{-1} at 10 K. (see Figure 11). The decrease in $\chi_M T$ upon lowering the temperature may conceivably be ascribed to a combination of the progressive depopulation of the excited Stark sublevels and the exchange interaction between the Dy^{III} ions.[3,9−12]

To probe the magnetization dynamics of the two new Dy^{III} compounds **1** and **3**, the temperature (2−30 K) and frequency dependence (163−1176 Hz) of the ac magnetic susceptibilities were measured in the absence of an applied dc magnetic field. Both compounds exhibit a frequency dependence in-phase (χ')

DOI: 10.1021/acs.inorgchem.5b00334
Inorg. Chem. 2015, 54, 8197−8206

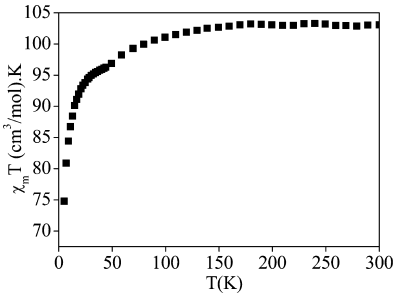

Figure 11. $\chi_M T$ vs T plot for complex **3**.

and out-of-phase (χ'') signal below ~8 K as shown in Figure 12. These data are indicative of the slow magnetization relaxation

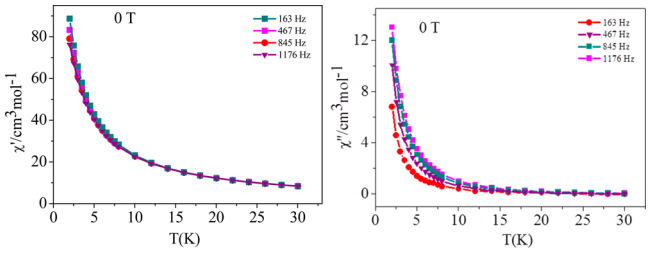

Figure 12. Temperature dependence of the in-phase (χ') and out-of-phase (χ'') ac susceptibility of **1** under zero dc field.

of an SMM with a small energy barrier for magnetization reversal. However, no maxima in the out-phase ac susceptibility data have been observed. This behavior is presumably due to the existence of a fast quantum tunneling relaxation of the magnetization (QTM) promoted by intermolecular dipolar interactions. To partially or fully suppress the quantum tunneling process, ac susceptibility measurements were performed under a static dc field of 0.5 T, where the frequency dependence in-phase (χ') and out-of-phase (χ'') signals below ~6 K reveals an enhancement of the maxima as shown in Figures 13 and 14 clearly suggesting a slow relaxation of magnetization. Another relaxation process at ~17 K was

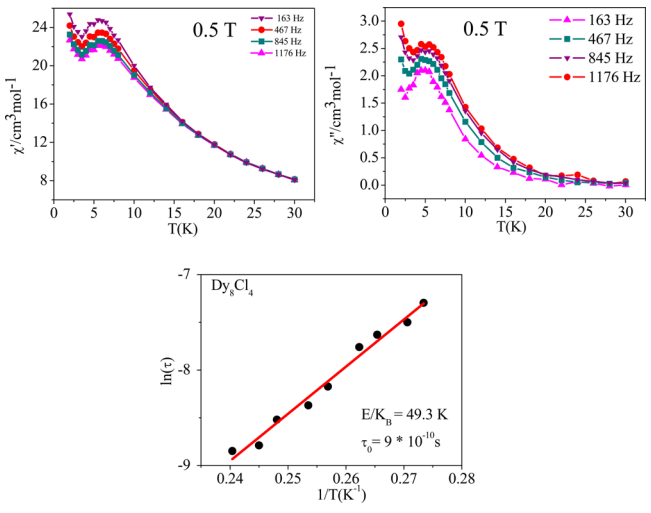

Figure 13. Temperature dependence of the in-phase (χ') and out-of-phase (χ'') ac susceptibility of **1** (Dy_8Cl_4) in the presence of an applied dc field of 0.5 T. Plot of ln(τ) vs 1/T. Solid line representing the fitting of the Arrhenius law.

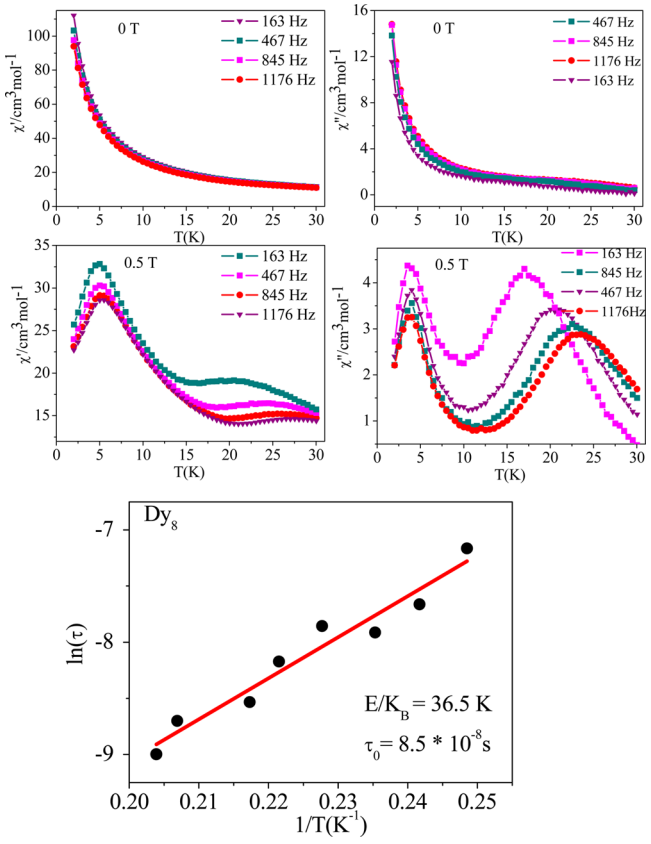

Figure 14. Temperature dependence of the in-phase (χ') and out-of-phase (χ'') ac susceptibility of **3** (Dy_8) under zero dc field and in the presence of an applied dc field of 0.5 T. Plot of ln(τ) vs 1/T. Solid line representing the fitting of the Arrhenius law.

observed for complex **3**. Such behavior of the complexes **1** and **3** most likely arises from predominant single-ion effects of the individual Dy^{III} centers in the octanuclear core exhibited by these molecules. Hence, both the octanuclear Dy^{III} complexes **1** and **3** can be considered as SMMs.

The spin disorder parameter $\phi = (\Delta T_P/T_P)/\Delta(\log f)$ (f denotes the frequency used in ac measurement) for **1** and **3** are greater than 0.1 and belong to a normal value for a super paramagnet ($\phi > 0.1$), and hence **1** and **3** both can be considered as SMM, ruling out the possibility of a spin glass state ($\phi \approx 0.01$).[16] The relaxation time τ extracted from the maximum of χ'' at different frequencies ($\tau = 1/\omega$) follows the Arrhenius law ($\tau = \tau_0 \exp(\Delta_{eff}/k_BT)$ where τ_0, Δ_{eff}, and k_B are the pre-exponential factor, the relaxation energy barrier, and the Boltzmann constant, respectively. The least-squares fitting of the experimental data as shown in Figures 13 and 14 affording an energy barrier Δ_{eff} = 49.3 K with a pre-exponential factor τ_0 = 9.0 × 10^{-10} s for **1** and Δ_{eff} = 36.5 K, τ_0 = 8.5 × 10^{-8} s for **3**, consistent with the expected τ_0 from 1 × 10^{-5} to 1 × 10^{-11} for SMMs.[9−12] The Δ_{eff} value obtained is higher than or comparable to that of other dysprosium complexes,[9,10,12] smaller than that for some complexes reported in the literature,[3,11] and listed in Table 1.

The dc magnetic data of Tb^{III} complex **2** reveals that the $\chi_M T$ value at 300 K is 88.15 cm^3 K mol^{-1}, which is somewhat smaller than the theoretical value of 94.48 cm^3 K mol^{-1} expected for eight noninteracting Tb^{III} ions ($^7F_6$, S = 5/2, L = 3, J = 15/2, g = 3/2: C = 11.81 cm^3 K mol^{-1}).[8] The $\chi_M T$ product remains practically similar upon further cooling, until it reaches a value

DOI: 10.1021/acs.inorgchem.5b00334
Inorg. Chem. 2015, 54, 8197−8206

Table 1. Structural and Magnetic Features of Selected Dy and Tb Complexes

lanthanide core and/or topology	magnetic behavior of individual lanthanides: Dy	magnetic behavior of individual lanthanides: Tb	references
Dy_8 butterfly-shaped	SMM	SMM	
Tb_8 butterfly-shaped	Δ_{eff} = 49.3 K	Δ_{eff} = 33.9 K	
Dy_8 core	$\tau_0 = 9.0 \times 10^{-10}$ s	$\tau_0 = 7.9 \times 10^{-8}$ s	this work
	Δ_{eff} = 36.5 K		
	$\tau_0 = 8.5 \times 10^{-8}$ s		
Dy_6 core	SMM	non-SMM	
Tb_6 core	Δ_{eff} = 46.2 K		17a
	$\tau_0 = 2.85 \times 10^{-7}$ s		
Dy_4 seesaw topology	SMM	non-SMM	
Tb_4 do	no energy barrier reported		17b
Dy_6 core	SMM	SMM	
Tb_6 core	Δ_{eff} = 3.8 K	Δ_{eff} = 4.8K	17c
	$\tau_0 = 7.89 \times 10^{-6}$ s	$\tau_o = 1.43 \times 10^{-6}$ s	
Ln_4 square grid topology	non-SMM	non-SMM	17d
Dy_4 square grids	SMM	non-SMM	
Tb_4 square grids	Δ_{eff} = 91 K		17e
	$\tau_0 = 4.5 \times 10^{-7}$ s		
Dy_2 core	SMM	non-SMM	
Tb_2 core	Δ_{eff} = 53.7 K		17f
	$\tau_0 = 1.3 \times 10^{-9}$ s		
Dy_4 core	SMM	non-SMM	
Tb_4 core	Δ_{eff} = 28 K		
	$\tau_0 = 1.7 \times 10^{-7}$ s		
			17g
Dy mononuclear complex	SMM	non-SMM	
	Δ_{eff} = 75 K		17h
Tb mononuclear	$\tau_0 = 4.21 \times 10^{-5}$ s		
Dy_5 core	SMM	Tb complex not reported	
trigonal bipyramidal	Δ_{eff} = 1.91 K		17i
	$\tau_0 = 1.01 \times 10^{-6}$ s		
Dy_4 core	SMM	non-SMM	
Tb_4 core	Δ_{eff} = 62.6 K		17j
	$\tau_0 = 8.7 \times 10^{-7}$ s		
Dy mononuclear chain structure	SMM	Tb complex not reported	17k
	Δ_{eff} = 23.95 K, $\tau_0 = 3.12 \times 10^{-9}$ s		
mononuclear Dy	SMM	Tb complex not reported	17l
	Δ_{eff} = 49.3 K		
	$\tau_0 = 4.8 \times 10^{-6}$ s		
1D polymer	Δ_{eff} = 48.86 K	non SMM	17m
	$\tau_0 = 6.88 \times 10^{-7}$ s		
1D Dy polymeric chain	SMM	Tb complex absent	17n
	no energy barrier reported		
Dy_6 triangular prism	SMM	Tb complex not reported	
Dy_8 tub conformation	Δ_{eff} = 76 K		17o
	$\tau_0 = 1.2 \times 10^{-6}$ s		
Dy 3D polymeric network	SMM	Tb complex not reported	
	Δ_{eff} = 44.2 K		17p
	$\tau_0 = 2.4 \times 10^{-8}$ s		
Dy_3 linear cluster	SMM	non-SMM	17q
Tb_3 similar topology	Δ_{eff} = 39.79 K		
	$\tau_0 = 1.07 \times 10^{-7}$ s		
Dy_4 butterfly arrangement	SMM	Tb complex not reported	17r
	Δ_{eff} = 6.25 K		
	$\tau_0 = 3.75 \times 10^{-5}$ s		
Dy_5 butterfly-shaped	SMM	Tb complex not reported	17s
	Δ_{eff} = 197 K		
	$\tau_0 = 3.2 \times 10^{-9}$ s		
Dy_{10} four fused Dy_3 triangles	SMM	Tb complex not reported	
	no energy barrier reported		17t
Dy_5 trigonal bipyramidal cluster	SMM	Tb complex not reported	17u
	Δ_{eff} = 5k		
	$\tau_0 = 8.7 \times 10^{-7}$ s		
dinuclear Dy complex	SMM	Tb complex not reported	
	Δ_{eff} = 56.6 ± 0.9 K		17v
	$\tau_0 = 1.0 \times 10^{-7}$ s		
Dy_7 disclike structure	SMM	Tb complex not reported	
	Δ_{eff} = 140 K		17w
	$\tau_0 = 7.2 \times 10^{-9}$ s		
Dy double-decker complex	SMM	SMM	17x
	Δ_{eff} = (32 ± 3) K	Δ_{eff} = (383 ± 37) K	
Tb similar topology	$\tau_0 = (1.4 \pm 0.4) \times 10^{-6}$ s	$\tau_0 = (1.3 \pm 1.3) \times 10^{-8}$ s	
Dy_7 metal-centered trigonal prismatic topology	SMM	non-SMM	17y
	Δ_{eff} = 1.7 K		
	$\tau_0 = 0.2 \times 10^{-6}$ s		
Tb_7 similar topology			
Dy_4 core	SMM	non-SMM	12b
Tb_4 core	no energy barrier reported		

of 88.1 cm^3 K mol^{-1} at 160 K. The $\chi_M T$ value slowly decreases with decreasing temperature to reach a value 65.24 cm^3 K mol^{-1} at 10 K as shown in Figure 15. The decrease in $\chi_M T$ upon lowering the temperature presumably can be ascribed to a combination of the progressive depopulation of the excited Stark sublevels and the exchange interaction between the Tb^{III} ions, albeit weak.

The magnetization dynamics of the Tb^{III} compound **2** was also studied in the temperature (2−300 K) and frequency dependence (163−1176 Hz) modes by measuring the ac magnetic susceptibilities in the absence of an applied dc magnetic field. It exhibits very weak frequency dependence response for both in-phase (χ') and out-of-phase (χ'') signals. Such an effect presumably can be ascribed due to fast quantum

DOI: 10.1021/acs.inorgchem.5b00334
Inorg. Chem. 2015, 54, 8197−8206

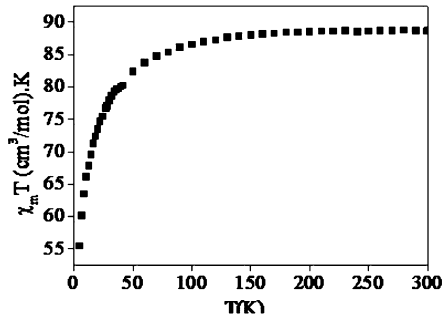

Figure 15. $\chi_M T$ vs T plot for complex **2**.

tunneling of relaxation. Hence, ac susceptibility measurements were performed under a static dc field of 0.5 T to suppress the relaxation due to quantum tunneling of magnetization. Figure 16 represents frequency dependence in-phase (χ') and out-of-

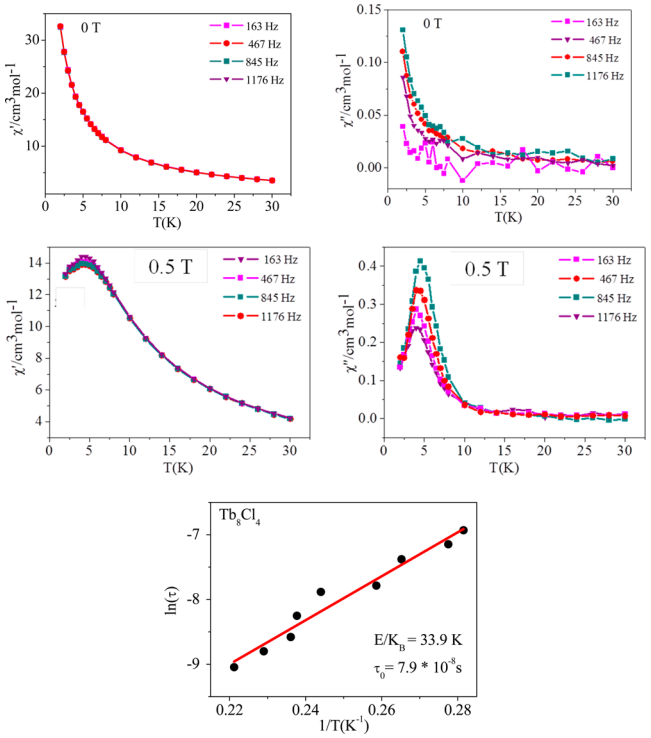

Figure 16. Temperature dependence of the in-phase (χ') and out-of-phase (χ'') ac susceptibility of **2** (**Tb_8Cl_4**) under zero dc field and in the presence of an applied dc field of 0.5 T. Plot of ln(τ) vs 1/T. Solid line representing the fitting of the Arrhenius law.

phase (χ'') signals with a maxima below 6 K clearly indicating a slow relaxation of magnetization by the {Tb^{III}_8} core. The relaxation time τ extracted from the maximum of χ'' at different frequencies ($\tau = 1/\omega$) follows the Arrhenius law ($\tau = \tau_0 \exp(\Delta_{eff}/k_BT)$. The least-squares fitting of the experimental data as shown in Figure 16 afford energy barrier Δ_{eff} = 33.9 K with a pre-exponential factor $\tau_0 = 7.9 \times 10^{-8}$ s for **2**. It is noteworthy here that Tb complexes with SMM behavior are not so common in the literature,[17] despite a plethora of reports on SMM behavior of lanthanide complexes.[17] Furthermore, the Δ_{eff} value obtained for complex **2** is significantly higher than these Tb^{III} complexes[17] listed in Table 1.

The magnetic measurement of **4** (**Nd_6**) complex shows that at 300 K the $\chi_m T$ is 6.19 cm^3 K mol^{-1}, which is smaller than the theoretical value of 9.6 cm^3 K mol^{-1} for six noninteracting Nd^{III} ions (Nd^{III}:$^4I_{9/2}$) due to crystal field splitting. When cooled, the $\chi_m T$ value decreases gradually and continuously and reaches a value of 3.17 cm^3 K mol^{-1} at 5 K as shown in Figure 17. This trend may indicate toward the very weak antiferromagnetic interaction between the Nd^{III} ions.

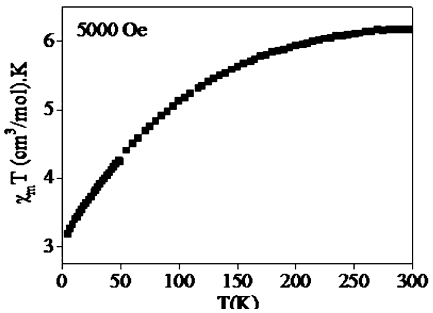

Figure 17. $\chi_m T$ vs T plot for the complex **4** (**Nd_6**) from 5−300 K measured under an applied dc field of 0.5 T.

CONCLUSIONS

Impetus for the work presented herein was to generate functional polynuclear lanthanide cage complexes using not-so-commonly used semi-rigid pyridyl−pyrazolyl-based ligands. Accordingly, we have successfully synthesized four polynuclear lanthanide cage complexes with {Dy^{III}_8} (**1**), {Tb^{III}_8} (**2**), {Dy^{III}_8} (**3**), and {Nd^{III}_6} (**4**) cores, which exhibit versatile molecular topologies. One of the most fascinating outcomes of this work is the construction of polynuclear lanthanide complexes with different coordination environments, which ultimately led to SMM behavior with slow magnetic relaxation for the two different {Dy^{III}_8} (**1** and **3**) and {Tb^{III}_8} (**2**) cores. It is imperative to note here that even with a plethora of polynuclear complexes in the literature, complex **2** represents one of those very few terbium complexes that exhibit SMM behavior. The synthetic approach illustrated in this work may open new opportunities to develop several new polynuclear lanthanide (III) complexes of different nuclearities and molecular topologies.

ASSOCIATED CONTENT

Supporting Information

The Supporting Information is available free of charge on the ACS Publications website at DOI: 10.1021/acs.inorgchem.5b00334. CIF files for the structures reported in this paper have been deposited with the Cambridge Crystallographic Data Centre (CCDC). Deposition numbers are CCDC 1027809 (**1**) and 1027811 (**2**), CCDC 1027808 (**3**), CCDC 1027810 (**4**). Copies of the data can be obtained, free of charge, on application to the CCDC, 12 Union Road, Cambridge CB2 1EZ, U.K. (fax 44 (1223) 336 033; e-mail deposit@ccdc.cam.ac.uk).

Keto−enol tautomerization of two ligands, perspective view of **2** with geometry around Tb center, solid-state luminescence study of complexes **1** and **3**, magnetic data points below 50 K, frequency-dependent in-phase and out-of phase components of ac susceptibility of compounds **1**, **2**, and **3**, crystal data and structure refinement parameters, and selected bond lengths and angles of complexes **1**−**4**. (PDF)

DOI: 10.1021/acs.inorgchem.5b00334
Inorg. Chem. 2015, 54, 8197−8206

X-ray crystallographic information for complex **1**. (CIF)
X-ray crystallographic information for complex **2**. (CIF)
X-ray crystallographic information for complex **3**. (CIF)
X-ray crystallographic information for complex **4**. (CIF)

AUTHOR INFORMATION

Corresponding Author

*E-mail: icrm@iacs.res.in.

Notes

The authors declare no competing financial interest.

ACKNOWLEDGMENTS

R.M. gratefully acknowledges Science and Engineering Research Board (SERB), India, for financial assistance (Project No. SR/S1/IC-65/2012). R.M. and K.M.F. acknowledge Indo-Swiss PEP joint research program (Project No. INT/SWISS/ISJRP/PEP/P-04/2012). S.K. is thankful to the founder director for the start-up grant. S.B. and B.P. are thankful to CSIR for fellowship, and the authors are thankful to Consortium for Scientific Research, Mumbai Centre, for helping in magnetic measurements.

REFERENCES

(1) (a) Stephenson, A.; Argent, S. P.; Riis-Johannessen, T.; Tidmarsh, I. S.; Ward, M. D. *J. Am. Chem. Soc.* **2011**, *133*, 858−870. (b) Tidmarsh, I. S.; Faust, T. B.; Adams, H.; Harding, L. P.; Russo, L.; Clegg, W.; Ward, M. D. *J. Am. Chem. Soc.* **2008**, *130*, 15167−15175. (c) Bell, Z. R.; Jeffery, J. C.; McCleverty, J. A.; Ward, M. D. *Angew. Chem., Int. Ed.* **2002**, *41*, 2515−2518.

(2) (a) Dearden, A. L.; Parsons, S.; Winpenny, R. E. P. *Angew. Chem., Int. Ed.* **2001**, *40*, 151−154. (b) Tolis, E. I.; Helliwell, M.; Langley, S.; Raftery, J.; Winpenny, R. E. P. *Angew. Chem., Int. Ed.* **2003**, *42*, 3804−3808.

(3) (a) Blagg, R. J.; Muryn, C. A.; McInnes, E. J. L; Tuna, F.; Winpenny, R. E. P. *Angew. Chem., Int. Ed.* **2011**, *50*, 6530−6533. (b) Tang, J. K.; Hewitt, I.; Madhu, N. T.; Chastanet, G.; Wernsdorfer, W.; Anson, C. E.; Benelli, C.; Sessoli, R.; Powell, A. K. *Angew. Chem., Int. Ed.* **2006**, *45*, 1729−1733.

(4) (a) Sessoli, R. *Angew. Chem., Int. Ed.* **2012**, *51*, 43−45. (b) Zheng, Y.-Z; Evangelisti, M.; Winpenny, R. E. P. *Angew. Chem., Int. Ed.* **2011**, *50*, 3692−3695.

(5) (a) Yang, X.; Schipper, D.; Jones, R. A.; Lytwak, L. A.; Holliday, B. J.; Huang, S. *J. Am. Chem. Soc.* **2013**, *135*, 8468−8471. (b) Sykes, D.; Ward, M. D. *Chem. Commun.* **2011**, *47*, 2279−2281. (c) Vandevyver, C. D. B; Chauvin, A. S.; Comby, S.; Bünzli, J. C. G. *Chem. Commun.* **2007**, 1716−1718. (d) Imbert, D.; Comby, S.; Chauvin, A. S.; Bünzli, J.C. G. *Chem. Commun.* **2005**, 1432−1434. (e) Driesen, K.; Vaes, K.; Cardinaels, T.; Goossens, K.; Gorller-Walrand, C.; Binnemans, K. *J. Phys. Chem. B* **2009**, *113*, 10575−10579. (f) Zaim, A.; Nozary, H.; Guenee, L.; Besnard, C.; Lemonnier, J. F.; Petoud, S.; Piguet, C. *Chem. - Eur. J.* **2012**, *18*, 7155−7168. (g) Lemonnier, J. F.; Guenee, L.; Beuchat, C.; Wesolowski, T. A.; Mukherjee, P.; Waldeck, D. H.; Gogick, K. A.; Petoud, S.; Piguet, C. *J. Am. Chem. Soc.* **2011**, *133*, 16219−16234. (h) Babel, L.; Hoang, T. N. Y; Nozary, H.; Salamanca, J.; Guenée, L.; Piguet, C. *Inorg. Chem.* **2014**, *53*, 3568−3578. (i) Starck, M.; Ziessel, R. *Dalton Trans.* **2012**, *41*, 13298. (j) Sykes, D.; Cankut, A. J.; Ali, N. M.; Stephenson, A.; Spall, S. J. P; Parker, S. C.; Weinstein, J. A.; Ward, M. D. *Dalton Trans.* **2014**, *43*, 6414−6428. (k) Ahmed, Z.; Iftikhar, K. *J. Phys. Chem. A* **2013**, *117*, 11183−11201. (l) Shi, X. M.; Tang, R. R.; Gu, G. L.; Huang, K. L. *Spectrochim. Acta, Part A* **2009**, *72*, 198−203. (m) Freire, R. O.; Vila-Nova, S. P.; Brunet, E.; Juanes, O.; Rodríguez-Ubis, J. C.; Alves, S., Jr. *Chem. Phys. Lett.* **2007**, *443*, 378−382.

(6) Bogani, L.; Wernsdorfer, W. *Nat. Mater.* **2008**, *7*, 179−186.

(7) Ritchie, C.; Moore, E. G.; Speldrich, M.; Kogerler, P.; Boskovic, C. *Angew. Chem., Int. Ed.* **2010**, *49*, 7702−7705.

(8) Benelli, C.; Gatteschi, D. *Chem. Rev.* **2002**, *102*, 2369−2388.

(9) (a) Yang, P.-P; Gao, X.-F; Song, H.-B; Zhang, S.; Mei, X.-L; Li, L.-C; Liao, D.-Z. *Inorg. Chem.* **2011**, *50*, 720−722. (b) Tian, H.; Zhao, L.; Guo, Y.-N; Guo, Y.; Tang, J.; Liu, Z. *Chem. Commun.* **2012**, *48*, 708−710. (c) Zangana, K. H.; Pineda, E. M.; Schnack, J.; Winpenny, R. E. P. *Dalton Trans.* **2013**, *42*, 14045−14048. (d) Chesman, A. S. R; Turner, D. R.; Moubaraki, B.; Murray, K. S.; Deacon, G. B.; Batten, S. R. *Dalton. Trans.* **2012**, *41*, 3751−3757.

(10) (a) Alexandropoulos, D. I.; Mukherjee, S.; Papatriantafyllopoulou, C.; Raptopoulou, C. P.; Psycharis, V.; Bekiari, V.; Christou, G.; Stamatatos, T. C. *Inorg. Chem.* **2011**, *50*, 11276−11278. (b) Canaj, A. B.; Tzimopoulos, D. I.; Philippidis, A.; Kostakis, G. E.; Milios, C. J. *Inorg. Chem.* **2012**, *51*, 7451−7453.

(11) (a) Boulon, M.-E; Cucinotta, G.; Luzon, J.; Degl'Innocenti, C.; Perfetti, M.; Bernot, K.; Calvez, G.; Caneschi, A.; Sessoli, R. *Angew. Chem., Int. Ed.* **2013**, *52*, 350−354. (b) Cucinotta, G.; Perfetti, M.; Luzon, J.; Etienne, M.; Car, P.-E; Caneschi, A.; Calvez, G.; Bernot, K.; Sessoli, R. *Angew. Chem., Int. Ed.* **2012**, *51*, 1606−1610.

(12) (a) Cao, D.-K.; Gu, Y.-W.; Feng, J.-Q.; Cai, Z.-S.; Ward, M. D. *Dalton Trans.* **2013**, *42*, 11436−11444. (b) Jami, A. K.; Baskar, V.; Sañudo, E. C. *Inorg. Chem.* **2013**, *52*, 2432−2438. (c) Joarder, B.; Chaudhari, A. K.; Rogez, G.; Ghosh, S. K. *Dalton. Trans.* **2012**, *41*, 7695−7699. (d) Xu, X.; Zhao, L.; Xu, G.-F; Guo, Y.-N; Tang, J.; Liu, Z. *Dalton. Trans.* **2011**, *40*, 6440−6444. (e) Li, D.-P; Wang, T.-W; Li, C.-H; Liu, D.-S; Li, Y.-Z; You, X.-Z. *Chem. Commun.* **2010**, *46*, 2929−2931. (f) Bi, Y.; Guo, Y.-N.; Zhao, L.; Guo, Y.; Lin, S.-Y.; Jiang, S.-D.; Tang, J.; Wang, B.-W.; Gao, S. *Chem. - Eur. J.* **2011**, *17*, 12476−12481. (g) She, S.-X.; Zaworotko, M. J.; Liu, W.; Zhang, Z.-X.; Li, Y. *CrystEngComm* **2013**, *15*, 5003−5006.

(13) (a) Ronson, T. K.; Adams, H.; Harding, L. P.; Pope, S. J. A; Sykes, D.; Faulkner, S.; Ward, M. D. *Dalton Trans.* **2007**, 1006−1022. (b) Metherell, A. J.; Ward, M. D. *Chem. Commun.* **2014**, *50*, 10979−10982.

(14) Bala, S.; Goswami, A.; Sengupta, S.; Ganguly, S.; Bhattacharya, S.; Khanra, S.; Mondal, R. *Cryst. Growth Des.* **2013**, *13*, 5068−5075.

(15) (a) Sheldrick, G. M. *SADABS;* Universität Gottingen: Gottingen, Germany, 2004. (b) Sheldrick, G. M. *Acta Crystallogr., Sect. A: Found. Crystallogr.* **2008**, *64*, 112−122.

(16) Mydosh, J. A. *Spin Glasses: An Experimental Introduction;* Taylor & Francis: London, U.K., 1993.

(17) (a) Das, S.; Hossain, S.; Dey, A.; Biswas, S.; Sutter, J. P.; Chandrasekhar, V. *Inorg. Chem.* **2014**, *53*, 5020−5028. (b) Goura, J.; Walsh, J. P.S; Tuna, F.; Chandrasekhar, V. *Inorg. Chem.* **2014**, *53*, 3385−3391. (c) Langley, S. K.; Moubaraki, B.; Murray, K. S. *Inorg. Chem.* **2012**, *51*, 3947−3949. (d) Biswas, S.; Das, S.; van Leusen, J.; Kögerler, P.; Chandrasekhar, V. *Eur. J. Inorg. Chem.* **2014**, *2014*, 4159−4167. (e) Anwar, M. U.; Thompson, L. K.; Dawe, L. N.; Habib, F.; Murugesu, M. *Chem. Commun.* **2012**, *48*, 4576−4578. (f) Liang, L.; Peng, G.; Li, G.; Lan, Y.; Powell, A. K.; Deng, H. *Dalton Trans.* **2012**, *41*, 5816−5823. (g) Zou, H. H.; Wang, R.; Chen, Z. L.; Liu, D. C.; Liang, F. P. *Dalton Trans.* **2014**, *43*, 2581−2587. (h) Na, B.; Zhang, X. J.; Shi, W.; Zhang, Y. Q.; Wang, B. W.; Gao, C.; Gao, S.; Cheng, P. *Chem. - Eur. J.* **2014**, *20*, 15975−15980. (i) Peng, J. B.; Kong, X. J.; Ren, Y. P.; Long, L. S.; Huang, R. B.; Zheng, L. S. *Inorg. Chem.* **2012**, *51*, 2186−2190. (j) Chandrasekhar, V.; Das, S.; Dey, A.; Hossain, S.; Sutter, J. P. *Inorg. Chem.* **2013**, *52*, 11956−11965. (k) Zeng, D.; Ren, M.; Bao, S.-S.; Zheng, L.-M. *Inorg. Chem.* **2014**, *53*, 795−801. (l) Liu, C. M.; Zhang, D. Q.; Zhu, D. B. *Inorg. Chem.* **2013**, *52*, 8933−8940. (m) Xu, W.; Zhou, Y.; Huang, D.; Xiong, W.; Su, M.; Wang, K.; Han, S.; Hong, M. *Cryst. Growth Des.* **2013**, *13*, 5420−5432. (n) Thiele-mann, D. T.; Klinger, M.; Wolf, T. J. A; Lan, Y.; Wernsdorfer, W.; Busse, M.; Roesky, P. W.; Unterreiner, A. N.; Powell, A. K.; Junk, P. C.; Deacon, G. B. *Inorg. Chem.* **2011**, *50*, 11990−12000. (o) Guo, Y. N.; Chen, X. U.; Xue, S.; Tang, J. *Inorg. Chem.* **2012**, *51*, 4035−4042. (p) Chen, Z.; Zhao, B.; Cheng, P.; Zhao, X. Q.; Shi, W.; Song, Y. *Inorg. Chem.* **2009**, *48*, 3493−3495. (q) Guo, F. S.; Liu, J. L.; Leng, J. D.; Meng, Z. S.; Lin, Z. J.; Tong, M. L.; Gao, S.; Ungur, L.; Chibotaru, L. F. *Chem. - Eur. J.* **2011**, *17*, 2458−2466. (r) Langley, S. K.; Chilton, N. F.; Gass, I. A.; Moubaraki, B.; Murray, K. S. *Dalton Trans.* **2011**, *40*,

DOI: 10.1021/acs.inorgchem.5b00334
Inorg. Chem. 2015, 54, 8197−8206

12656−12659. (s) Tian, H.; Zhao, L.; Lin, H.; Tang, J.; Li, G. *Chem. - Eur. J.* **2013**, *19*, 13235−13241. (t) Ke, H.; Xu, G. F.; Zhao, L.; Tang, J.; Zhang, X. Y.; Zhang, H. J. *Chem. - Eur. J.* **2009**, *15*, 10335−10338. (u) Shi, P. F.; Zheng, Y. Z.; Zhao, X. Q.; Xiong, G.; Zhao, B.; Wan, F. F.; Cheng, P. *Chem. - Eur. J.* **2012**, *18*, 15086−15091. (v) Layfield, R. A.; McDouall, J. J. W; Sulway, S. A.; Tuna, F.; Collison, D.; Winpenny, R. E. P. *Chem. - Eur. J.* **2010**, *16*, 4442−4446. (w) Sharples, J. W.; Zheng, Y. Z.; Tuna, F.; McInnes, E. J. L; Collison, D. *Chem. Commun.* **2011**, *47*, 7650−7652. (x) Gimenez-Agullo, N.; de Pipaon, C. S.; Adriaenssens, L.; Filibian, M.; Martinez-Belmonte, M.; Escudero-Adan, E. C.; Carretta, P.; Ballester, P.; Galan-Mascaros, J. R. *Chem. - Eur. J.* **2014**, *20*, 12817−12825. (y) Mazarakioti, E. C.; Poole, K. M.; Cunha-Silva, L.; Christou, G.; Stamatatos, T. C. *Dalton Trans.* **2014**, *43*, 11456−11460.

DOI: 10.1021/acs.inorgchem.5b00334
Inorg. Chem. 2015, 54, 8197−8206